View Online / Journal Homepage / Table of Contents for this issue
Dynamic Article Links

Journal of Materials Chemistry

Cite this: J. Mater. Chem., 2012, 22, 470

www.rsc.org/materials

PAPER

Bio-modified Fe_3O_4 core/Au shell nanoparticles for targeting and multimodal imaging of cancer cells†

Ting Zhou, Baoyan Wu and Da Xing*

Received 2nd August 2011, Accepted 10th October 2011
DOI: 10.1039/c1jm13692e

Published on 09 November 2011 on http://pubs.rsc.org | doi:10.1039/C1JM13692E
Downloaded by Xiamen University on 13 December 2011

Multimodal imaging based on complementary detection principles has great potential for improving the accuracy of tumor diagnosis. Fe_3O_4 core/Au shell nanoparticles (Fe_3O_4@Au NPs) can be used as an effective multimodal contrast agent due to combining the advantageous and highly complementary features of the Fe_3O_4 core and gold shell. In the present work, we have developed a novel Fe_3O_4@Au NP based probe for targeting and multimodal imaging of cancer cells. The prepared Fe_3O_4@Au NPs have been characterized by transmission electron microscopy (TEM), visible spectra and SERS. The potential use of the prepared Fe_3O_4@Au NPs as a multimodal contrast probe for magnetic resonance imaging (MRI), microwave-induced thermoacoustic imaging and photoacoustic imaging was then evaluated. Importantly, when conjugated with a cancer cell targeted molecular and fluorescent dye, the Fe_3O_4@Au NPs could be internalized by the corresponding cancer cells selectively and sensitively, and fluorescence imaging was realized at the same time. The bio-modified Fe_3O_4@Au NPs incorporating multiple functionalities into one single nano-structured system can be effectively used for targeting and multimodal imaging of cancer cells simultaneously.

Introduction

Noninvasive imaging of cancer with various modalities to present the tumor anatomical structure as well as its metabolism and biochemistry is crucial in cancer early detection and localization.[1] Existing clinical imaging modalities include computed tomography (CT), magnetic resonance imaging (MRI), positron emission tomography (PET), optical fluorescence, and ultrasound imaging. Each of them possesses characteristic strengths and weaknesses, but none of them are capable of providing complete structural and functional information independently or remarkably superior to all other methods.[2,3] So it is highly desirable to integrate the strengths of individual modalities for comprehensive information to improve early and accurate detection of tumors. However, on the one hand, detection with several imaging modalities needs injection of various contrast agents, which is time-consuming and painful for patients. On the other hand, different contrast agents may influence each other. The emergence of multimodal contrast agents that are capable of generating contrast in different ways by several components will solve these problems.[4–6] They need to be injected only once to complete various imaging modalities. Therefore multimodal contrast agents can avoid the influence resulted from different contrast agents.

Recently, various types of hybrid nanoparticles have been used for multimodal imaging.[7–11] Hybrid nanoparticles incorporating several components into one single nano-structured system integrate the strengths of individual components. So they are ideal multimodal contrast agents. They are usually constructed by combining the components of various nanoparticles together or modifying the single component nanoparticles with some other materials. Two or more imaging components are encapsulated into a silicon nanoshell, lipid or some other organic compounds.[12–15] Fluorescent dyes or some other molecules used for imaging are modified on the surface of nanoparticles.[16,17] Two or more kinds of nanoparticles are connected with covalent or non-covalent linkage.[18,19] Multimodal contrast agents which are formed by encapsulating multiple nanoparticles together have short circulation time in blood in response to their large particle diameters.[20,21] And the hybrid nanoparticles constructed by non-covalent linkage are not stable enough.

Fe_3O_4 core/Au shell nanoparticles (Fe_3O_4@Au NPs) are hybrid nanoparticles with gold shell directly coated onto the Fe_3O_4 core. Compared with most of the existing multimodal contrast agents, it has a very stable structure, controlled particle size and smooth surface. In addition, it has highly complementary advantages for various biomedical applications based on the performance of both the Fe_3O_4 core and gold shell. Fe_3O_4 nanoparticles (Fe_3O_4 NPs) have been used for various biomedical applications, such as MRI, magnetic separation for their magnetic property, and microwave-induced thermoacoustic for their strong absorption of microwave.[22–24] Au nanoparticles (Au NPs) have been extensively used in biological applications due to

MOE key Laboratory of Laser Life Science & Institute of Laser Life Science, College of Biophotonics, South China Normal University, Guangzhou, 510631, China. E-mail: xingda@scnu.edu.cn; Fax: +86-20 8521-6052; Tel: +86-20 8521-0089

† Electronic supplementary information (ESI) available. See DOI: 10.1039/c1jm13692e

This journal is © The Royal Society of Chemistry 2012

Published on 09 November 2011 on http://pubs.rsc.org | doi:10.1039/C1JM13692E
Downloaded by Xiamen University on 13 December 2011

their biocompatibility and absorption properties, which make them good contrast agents for CT and photoacoustic imaging. Their rich history of surface chemistry can also be used for subsequent treatment with some useful chemical or biological molecules. Consequently, Fe_3O_4@Au NPs have potential uses as a multimodal contrast agent for MRI, CT, microwave-induced thermoacoustic, photoacoustic imaging and magnetomotive photoacoustic imaging.[7,25,26] Importantly, when conjugated with a fluorescent dye, they can also be used for fluorescence imaging, which has a much higher sensitivity than the above-mentioned imaging modalities. With the Fe_3O_4@Au NPs, we can identify the specific location of tumor in the body before surgery with a MRI, microwave-induced thermoacoustic imaging or photoacoustic imaging scan, and then use fluorescence imaging to find and remove all parts of the tumor during the operation.

Contrast agents targeting tumors may achieve a better imaging effect but with fewer and less severe side effects.[27] Most of the reported nano-probes for tumor imaging are accumulated in tumor tissue through the EPR (Enhanced Permeability and Retention) effect[28] or magnetic tumor targeting with external magnets. The EPR effect helps to carry the nanoparticles and makes them spread inside the cancer tissue, but it is passively targeted and limited to hyper-proliferative tissues, so that the targeting effect during very early stages of cancer is insufficient.[29,30] Magnetic tumor targeting is incapable of targeting areas within deep tissues, mainly because of a rapid attenuation of the magnetic field magnitude away from the magnets.[31] Nevertheless, targeting nanoparticles labeled with targeting molecule are internalized into cells mainly through the ligand–receptor or antibody–antigen mediated endocytosis pathway.[32–34] Accordingly, coupling the nanoparticle to a targeting molecule which recognizes tumor-associated antigens is a rational strategy to increase the target selectivity of cancer cells and provide safer and more effective diagnosis.[14,35–37] In our study, integrin $\alpha_v\beta_3$ (23C6) mono-clonal antibody (integrin $\alpha_v\beta_3$ mAb) was used as the targeting molecule. Integrin $\alpha_v\beta_3$ serves as a promising cancer cell targeting marker, since it is not readily detectable in quiescent vessels but has high expression in various cancer cells (glioma, melanoma and ovarian) and tumor neovasculature compared to normal tissues.[38,39]

Herein, Fe_3O_4@Au NPs were synthesized and developed as a multimodal imaging probe for MRI, microwave-induced thermoacoustic tomography and photoacoustic imaging for their versatile properties. After we conjugated the Fe_3O_4@Au NPs with fluorescein-labeled integrin $\alpha_v\beta_3$ mAb, they could also be selectively and sensitively internalized into the integrin $\alpha_v\beta_3$-positive cancer cell, and fluorescence imaging was realized at the same time. In brief, the bio-modified Fe_3O_4@Au NPs can be used as a multifunctional probe for targeting and multimodal imaging of cancer cells simultaneously. Due to broad applications for cancer imaging, this novel imaging probe is expected to lead to significant development in cancer diagnosis.

Experimental section

Synthesis of core–shell Fe_3O_4@Au NPs

The Fe_3O_4 nanoparticles were prepared using a modified chemical co-precipitation protocol.[40] Briefly, 2.703 g of $FeCl_3 \cdot 6H_2O$ and 0.998 g of $FeCl_2 \cdot 4H_2O$ were dissolved in 100 mL deionized water. Under nitrogen atmosphere, ammonia was added with vigorous stirring till the pH reached 9.0–9.5. The solution was then stirred continuously for 15 minutes at room temperature. After amination the mixture was heated to 80 °C and kept stirring for 30 minutes.

A 2 mL portion of the as-prepared Fe_3O_4 NPs solution was washed with sodium citrate solution (10 mM) for three times and then dissolved in 100 mL of that sodium citrate solution. After being sonicated for several hours to exchange absorbed OH^- with citrate anions, the solution was put into a 250 mL flask and heated to 70 °C under mild stirring. 10 mL of chloroauric acid hydrated was dropped into the solution and allowed to react for 30 minutes under vigorous stirring. Then the water bath was removed and the suspension was cooled to room temperature for 1 hour under continuous stirring. These core–shell Fe_3O_4@Au NPs were separated from free gold nanoparticles by an external magnet and redispersed in deionized water, then stored in a refrigerator at 4 °C.

Characterization experiments

To examine the size of Fe_3O_4 and Fe_3O_4@Au nanoparticles, the samples were observed using a HITACHI H-300 transmission electron microscope (TEM) with parameters of 70 kV voltage and 70 pA current.

The optical absorbance characteristics of various samples were investigated by visible absorption spectra (Lambda-35 UV-Vis spectrophotometer, Perkin-Elmer, USA).

Raman spectroscopy was used to detect the surface-enhanced Raman scattering (SERS) of 4,4′-dipyridyl bonded to Fe_3O_4 NPs, Au NPs and Fe_3O_4@Au NPs. 5 μL of 4,4′-dipyridyl was added to 1 mL of Fe_3O_4 NPs, Au NPs and Fe_3O_4@Au NPs, respectively, and all these nanoparticles were 1 mM in concentration. An argon ion laser (514.5 nm) was used for excitation in combination with a 40× objective of an Olympus BX-41 microscope, an Acton spectro@2300i spectrometer system (Princeton Acton, USA) and a Pixis 256 CCD detector (Princeton Acton, USA). After focusing at the center of the capillary, the Raman spectrum of the samples with a resolution of 2 cm^{-1} (10 mW power, 20 s collection time) was recorded.

Modified Fe_3O_4@Au NPs with FITC-labeled integrin $\alpha_v\beta_3$ mAb

Integrin $\alpha_v\beta_3$ mAb was labeled with FITC (Fluorescein isothiocyanate) by the procedures according to Ou *et al.*[41] Briefly, a 400 μL solution of integrin $\alpha_v\beta_3$ mAb at a concentration of 40 nM in standard PBS was mixed with FITC (0.1 mg mL^{-1}, 100 μL) dissolved in DMSO. After incubating the mixture for several hours at 4 °C, protected from illumination, the conjugated integrin $\alpha_v\beta_3$ mAb–FITC was filtered through 1 kDa filters (Millipore) to remove the excess FITC.

100 μL of 1 mg mL^{-1} mPEG-SH (methoxy-polyethylene glycol-thiol, MW 5000) was added into 1 mL of the as-prepared Fe_3O_4@Au solution. After the solution was sonicated for 30 minutes, 100 μL of 1 mM 11-MUA ($SHC_{11}H_{22}CO_2H$) dissolved in DMSO was added into it. Then the solution was mixed and sonicated for several hours at room temperature to accelerate the reaction. Excess mPEG-SH and 11-MUA were removed in the presence of an external magnet and the resulting particles

Published on 09 November 2011 on http://pubs.rsc.org | doi:10.1039/C1JM13692E
Downloaded by Xiamen University on 13 December 2011

were redispersed in deionized water. Then 100 μL of 5 mM EDC (1-ethyl-3-(3-dimethylaminopropyl)carbodiimide hydrochloride) and 100 μL of 5 mM NHS (*N*-hydroxysuccinimide) were added to the resultant solution in succession and reacted at 4 °C overnight. Excess EDC and NHS were also removed by an external magnet and the resulting particles were redispersed in standard PBS. 100 μL of as-prepared FITC labeled integrin $\alpha_v\beta_3$ mAb was further added to the carboxylated Fe_3O_4@Au solution and reacted for 3 hours at 4 °C, protected from illumination. The nanoparticles were magnetically extracted from the supernatant, washed with PBS two times, redispersed in 1 mL PBS and then stored in a refrigerator at 4 °C, protected from illumination.

Magnetic resonance imaging

Fe_3O_4 NP and Fe_3O_4@Au NP samples with different concentrations were prepared by diluting the synthesized nanoparticles with deionized water (resistance 18.2 MΩ). Samples of dilute Fe_3O_4 NPs and Fe_3O_4@Au NPs were filled in Eppendorf tubes and then embedded in an agar phantom. MRI was performed with a 1.5 T Imager (GE Signa HD, 1.5 T MR, GE Healthcare, Milwaukee, WI, USA) and a 12.7 cm receive-only knee coil. MR coronal images were scanned using a fast spin echo T_2 sequence (repetition time (ms)/echo time (ms) = 4000/108, 16 echo train length) and a spin-echo T_1 sequence (repetition time (ms)/echo time (ms) = 500/17.9). Images were obtained with a matrix size of 256 × 256. Two measurements were acquired at the section thickness of 2 mm and field view of 13 × 13 cm^2. The region of interest (ROI) for signal intensity (SI) measurement was 38 mm^2. Twelve ROIs were randomly selected and measured in each tube. The specific relaxivity values of R were calculated through the curve fitting of $1/T_2$ (s^{-1}) *vs.* the Fe concentration (mM) as the slope of the resulting linear plot.

Microwave-induced thermoacoustic signal of Fe_3O_4@Au NPs

100 μL of deionized water and Fe_3O_4@Au NPs with iron concentrations of 2.5, 5.0, 10 and 20 mM were put into a silicon tube with a diameter of 0.8 mm to detect their microwave-induced thermoacoustic signals, respectively. The microwave generator at 6 GHz (BW-6000HPT, China) transmitted out short pulse microwave with a pulse width of 0.5 μs and an external trigger repetition rate of 10 Hz. The data acquisition system for thermoacoustic CT included a piezoelectric transducer (Doppler Ltd., Central frequency: 2.5 MHz) and a high-speed digital data-acquisition card (PCI-GPIB, NI, USA). The piezoelectric transducer was used for detecting the original thermoacoustic signals. The device was designed according to Nie *et al.*[24]

Photoacoustic signal of Fe_3O_4@Au NPs

100 μL of Fe_3O_4@Au NPs with gold concentrations of 2, 4, 8 and 16 mM were put into a silicon tube with a diameter of 0.8 mm to detect their photoacoustic signals, respectively. An Nd:YAG pumped laser (wavelength: 532 nm, pulse width: 7 ns, and repetition rate: 15 Hz) provides laser pulses to irradiate the samples for generating photoacoustic signals. The ultrasound transducer with 75 MHz center frequency and 65% fractional bandwidth was used to receive the photoacoustic signals. The photoacoustic device was designed according to Xiang *et al.*[42]

Cell culture

U87-MG human glioblastoma cancer cells and MCF-7 human breast cancer cells were cultured in Eagle's minimal essential medium (EMEM) and Dulbecco's modified Eagle's medium (DMEM), respectively. The media were supplemented with 10% fetal bovine serum (FBS) and 1% penicillin–streptomycin in 5% CO_2, 95% air at 37 °C in a humidified incubator.

Selective imaging of cancer cells

After incubating the cells of 500 μL with bio-modified Fe_3O_4@Au NPs at 37 °C (5% CO_2) for 1 hour, the cells were rinsed with fresh culture medium. A 500 μL of U87-MG cells was pre-blocked by integrin $\alpha_v\beta_3$ mAb, and then was treated as above. These cells were imaged by a commercial laser scanning microscope (LSM510/ConfoCor2) combination system (Zeiss, Germany) equipped with a Plan-Neo fluar 40×/1.3 NA oil DIC objective. The nano-probe was excited at 488 nm with an Ar-ion laser (reflected by a beam splitter HFT 488 nm) and the fluorescence emission was recorded through a 500–550 nm IR band-pass filter.

Quantification of fluorescence intensity

To quantify the fluorescence intensity, U87-MG cells and MCF-7 cells were treated as the imaging experiments, then rinsed with PBS, and harvested with trypsin. Cells under different treatments were washed and resuspended in ice-cold PBS. The fluorescence histogram of cells was obtained from 10 000 cells by flow cytometry (Becton Dickinson FACScan).

Result and discussion

Fabrication of bio-modified Fe_3O_4@Au NPs

The synthesis of the high performance core/shell Fe_3O_4@Au NPs involved two phases. In the first phase, Fe_3O_4 NPs were synthesized through the co-precipitation of ferric chloride and ferrous chloride by ammonia. In the second phase, gold was coated onto the Fe_3O_4 NPs through the reduction of $HAuCl_4$ by the citrate absorbed on the surface of Fe_3O_4.

Fig. 1 is the schematic procedure for fabrication of the bio-modified multifunctional nanoparticles. mPEG-SH was immobilized on the surface of gold shell *via* the formation of stable, covalent gold–thiol linkages. It suppresses immunogenic responses, thus prolongs the circulation time of the nanoparticles and allows sufficient time for them to localize in different organs.[43] The mPEG-SH functionalized Fe_3O_4@Au NPs were then conjugated with 11-MUA to cap them with carboxy groups. Subsequently, using EDC/NHS chemistry, the tumor-targeted multimodality contrast agents were thus constructed by fabricating the FITC-labeled integrin $\alpha_v\beta_3$ mAb on the surface of Fe_3O_4@Au NPs capped with carboxy groups.

Characterization of bio-modified Fe_3O_4@Au NPs

The TEM micrographs of Fe_3O_4 NPs and Fe_3O_4@Au NPs are illustrated in Fig. 2A and B, respectively. The size of Fe_3O_4@Au NPs was obviously increased since the particles had been coated by gold. And the dispersibility of Fe_3O_4@Au NPs was better than

 This journal is © The Royal Society of Chemistry 2012

Published on 09 November 2011 on http://pubs.rsc.org | doi:10.1039/C1JM13692E
Downloaded by Xiamen University on 13 December 2011

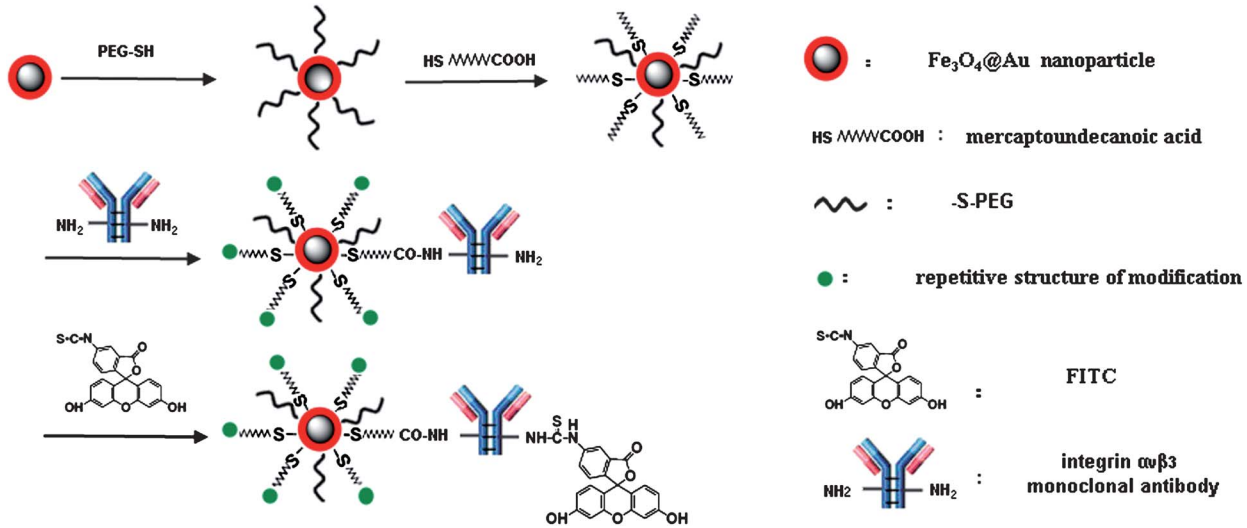

Fig. 1 An illustration of the procedures for producing the integrin $\alpha_v\beta_3$ mAb–FITC modified Fe_3O_4@Au NPs.

Fe_3O_4 NPs without gold shell, reflecting the enhanced stability resulting from the gold shell. Fig. 2C shows the visible spectra of Fe_3O_4 NPs, Au NPs of 13 nm, Fe_3O_4@Au NPs with and without purification. Fe_3O_4@Au NPs reached an absorption peak at 526 nm, which is the characteristic absorbance of gold nanoparticles. The red-shifting in the hybrid nanoparticles was in agreement with their relatively larger diameters. After the prepared Fe_3O_4@Au NPs were purified by removing free gold NPs with an external magnet, and then centrifuged to remove uncoated Fe_3O_4 NPs, the absorption peak became more evident. In addition, similar to Fe_3O_4 NPs, the absorption of Fe_3O_4@Au NPs in the range of 400–500 nm was much stronger than that of Au NPs, which was most likely a consequence of the existence of a few uncoated Fe_3O_4 NPs. From the picture of Fig. 2C, we can clearly see the color change of Fe_3O_4 NPs before and after gold coating. The red color of the resulting Fe_3O_4@Au NPs indicated that they had inherited the colorimetric character of Au NPs. A small amount of gold nanoparticles without iron oxide nanoparticles (2.9% of the total Au concentration, see ESI†), which was reflected by the light pink color remaining in the solution, was separated from magnetic Fe_3O_4@Au NPs with an external magnet.

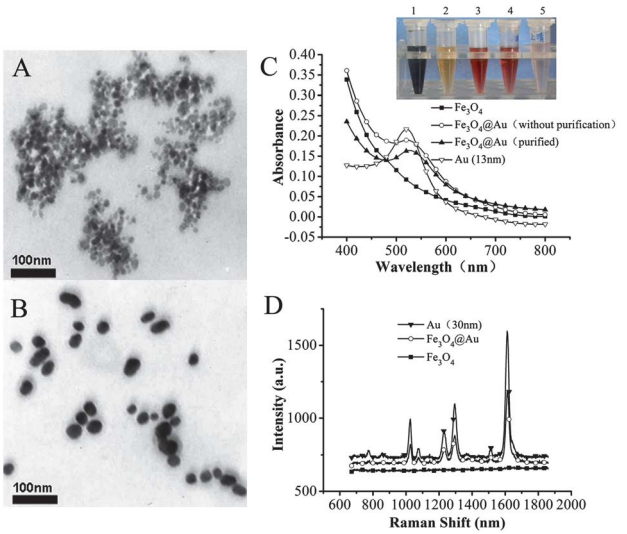

Fig. 2 TEM pictures of (A) Fe_3O_4 nanoparticles with an average diameter of ~10 nm and (B) Fe_3O_4@Au NPs with an average diameter of 30–50 nm; (C) visible absorbance spectra of Fe_3O_4 NPs, Au NPs (13 nm), Fe_3O_4@Au NPs with and without purification and color comparison (above) of 50 mM Fe_3O_4 NPs (1), 1 mM Fe_3O_4 NPs (2), Fe_3O_4@Au NPs without (3) and with purification (4) and the supernatant after getting rid of the nanoparticles by an external magnet (5); (D) SERS spectra measured from 4,4′-dipyridyl bonded to Au NPs (30 nm), Fe_3O_4 NPs and Fe_3O_4@Au NPs separately.

Surface-enhanced Raman scattering (SERS) is a surface sensitive technique that results in strong enhancement of Raman scattering signals by molecules absorbed on the surfaces of gold nanoparticles.[44] The Raman signal of 4,4′-dipyridyl is too weak to distinguish. But when 4,4′-dipyridyl was absorbed on the surface of Au NPs and Fe_3O_4@Au NPs, as shown in Fig. 2D, the SERS effect made the Raman signals become strong enough to detect. When absorbed on the surface of Fe_3O_4 nanoparticles, 4,4′-dipyridyl did not have the SERS effect. It is thus concluded that the SERS effect caused by Fe_3O_4@Au NPs must be from the gold shell. To sum up, the TEM photographs, visible spectra and SERS results all indicate the formation of a gold coating on the surface of Fe_3O_4 NPs.

Multimodal imaging using Fe_3O_4@Au NPs

As a common clinical imaging modality, MRI is a noninvasive imaging tool which offers high resolution and images tissues deeper than most optical imaging modalities.[45] To demonstrate the potential use as an enhanced MRI contrast agent, we examined the MR contrast effect of Fe_3O_4@Au NPs in comparison with that of free Fe_3O_4 NPs with an equivalent iron concentration. As shown in Fig. 3A, Fe_3O_4@Au NPs generate enhanced MR contrast on T_2 proton relaxation time weighted sequences. The T_2-weighted MR images of both Fe_3O_4 NPs and Fe_3O_4@Au NPs became darker as the concentrations of the probes increased. The images of Fe_3O_4@Au NPs were slightly

Published on 09 November 2011 on http://pubs.rsc.org | doi:10.1039/C1JM13692E
Downloaded by Xiamen University on 13 December 2011

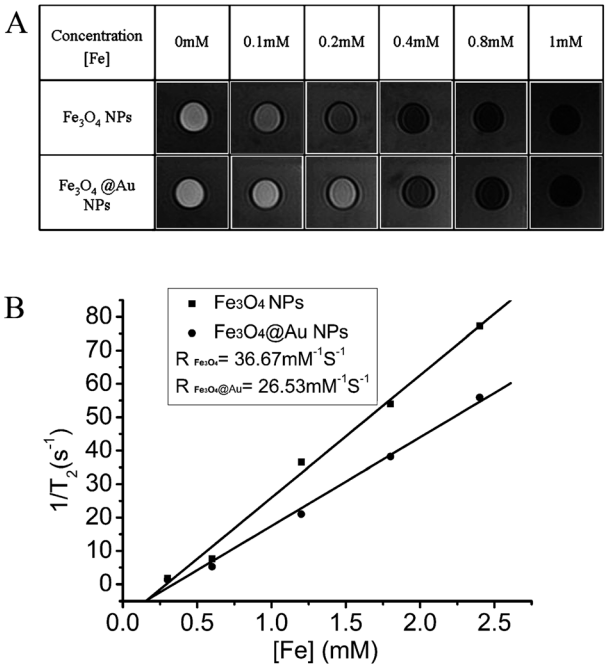

Fig. 3 (A) T_2-Weighted MR images of bare Fe_3O_4 NPs and Fe_3O_4@Au NPs at various [Fe] dilutions. Signal strength is indicated by the darkness of the images. (B) T_2-Relaxivity plots of aqueous suspension of Fe_3O_4 NPs and Fe_3O_4@Au NPs.

lighter than those of Fe_3O_4 NPs without gold nanoshell coating indicating the weaker MR signals of Fe_3O_4@Au NPs. Analogously, Fig. 3B shows that the relaxivity value R of Fe_3O_4@Au NPs is determined to be 26.53 mM^{-1} s^{-1}, which is slightly lower than that of Fe_3O_4 NPs (36.67 mM^{-1} s^{-1}). This is because the magnetic properties of Fe_3O_4@Au NPs are weaker than those of Fe_3O_4 NPs due to the gold nanoshell coating. By comparing with previously reported Fe_3O_4/Au nanocomposites, such as Au–Fe_3O_4 dumbbell nanoparticles[19] and iron oxide–gold hybrid NPs with an organic gap,[7] Fe_3O_4@Au NPs at an equivalent iron concentration have a similar MR contrast effect. Moreover, compared with the most clinically used Gd(III) complexes, the nanoparticle-based agents have a longer residence time in the vascular system, so that they could greatly increase the imaging time.[46] And compared with the commercial T_2-weighted contrast agents (such as dextran-coated iron oxide NPs), the Fe_3O_4@Au NPs have better stability and a richer history of surface chemistry due to the gold coating.

Microwave-induced thermoacoustic tomography, which offers deep tissue penetration and high spatial resolution, is a hybrid of microwave imaging and ultrasound imaging.[47] To confirm Fe_3O_4@Au NPs can be used as an effective contrast agent for microwave-induced thermoacoustic tomography, we detected the thermoacoustic signals of Fe_3O_4@Au NPs at various iron concentrations. The thermoacoustic signals generated by deionized water and Fe_3O_4@Au NP solutions are displayed in Fig. 4A. The signals increased evidently with the increase of the iron concentration, and the intensity was 180% of that of water when the iron concentration reached 20 mM. The data indicate that the thermoacoustic signal produced by Fe_3O_4@Au NPs solution is in linear relationship with iron concentrations (R^2 = 0.987, Fig. 4B). The observed oscillation in the thermoacoustic signal was likely a result of the limited bandwidth of the transducer. These results suggest that the Fe_3O_4@Au NPs possessed microwave absorption property and could generate the thermoacoustic signal when irradiated with pulsed microwave. As Nie *et al.* reported,[24] when the intensity of the thermoacoustic signal produced by Fe_3O_4 NPs was about 1.5 times that of water, a high-contrast image could be reconstructed. Therefore, we conclude that Fe_3O_4@Au NPs can be used as a potential contrast agent for microwave-induced thermoacoustic tomography.

Compared with some purely optical imaging, such as fluorescence imaging, photoacoustic imaging can provide an image in a region up to several centimetres deep in biological tissue. In the mean time, photoacoustic imaging is more economical and convenient to operate than MRI.[7,48,49] Au NPs have been reported as an ideal contrast agent for photoacoustic imaging owing to their strong optical absorption near 532 nm wavelength.[50,51] In order to determine if Fe_3O_4@Au NPs can be used as a contrast agent for photoacoustic imaging, the photoacoustic signal of Fe_3O_4@Au NPs with various gold concentrations was detected using a 532 nm pulse laser as the irradiation source. The choice of the laser wavelength was based on the absorbance spectra of Fe_3O_4@Au NPs shown in Fig. 2C, which suggests that the nanoparticles have a strong absorption at 532 nm. The photoacoustic signals generated by the Fe_3O_4@Au NP solutions were summarized in Fig. 5A. As we expected, the intensity of the photoacoustic signal was linearly correlated with the gold concentrations (R^2 = 0.993, Fig. 5B). All the results indicate that

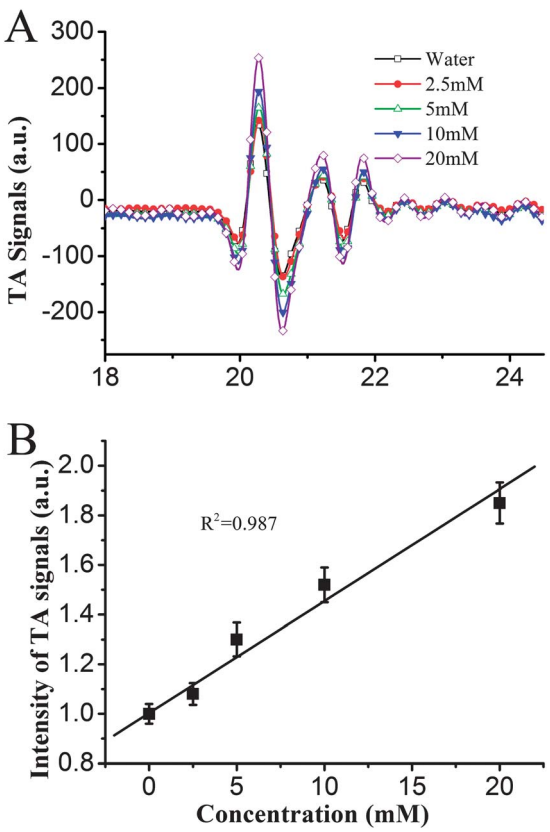

Fig. 4 (A) Microwave-induced thermoacoustic signals of Fe_3O_4@Au NPs at various [Fe] dilutions and (B) linear fitting of thermoacoustic signal intensity under the corresponding iron concentrations.

This journal is © The Royal Society of Chemistry 2012

Published on 09 November 2011 on http://pubs.rsc.org | doi:10.1039/C1JM13692E
Downloaded by Xiamen University on 13 December 2011

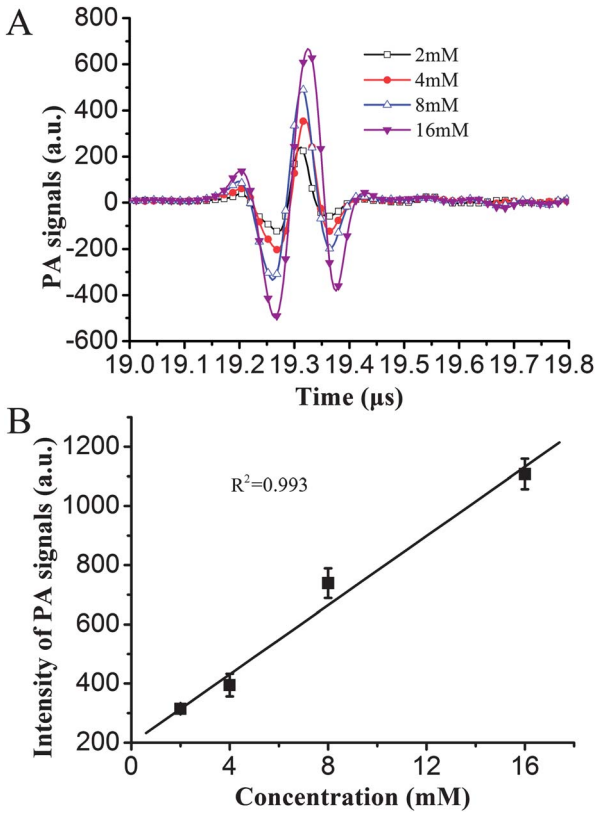

Fig. 5 (A) Photoacoustic signals of Fe_3O_4@Au NPs at various [Au] dilutions and (B) linear fitting of photoacoustic signal intensity under the corresponding gold concentrations.

Fe_3O_4@Au NPs are a potential contrast agent for photoacoustic imaging.

The above results show that Fe_3O_4@Au NPs can be used as probes for MRI, microwave-induced thermoacoustic tomography and photoacoustic imaging.

Selective fluorescence imaging of cancer cells with biomodified Fe_3O_4@Au NPs

Fluorescence imaging has higher sensitivity than all of the above-mentioned imaging modalities. Furthermore, compared to MRI and radio imaging, it is more convenient to monitor multiple biological processes simultaneously and in real time.[52] Antibody-conjugated nanoparticles can be selectively internalized into cells highly expressing the corresponding antigen through the antigen–antibody mediated endocytosis pathway. After being modified with integrin $\alpha_v\beta_3$ mAb, Fe_3O_4@Au NPs can be specifically internalized into integrin $\alpha_v\beta_3$-positive cells. When FITC is labeled on them, they are useful for fluorescent imaging. To investigate the tumor targeting and fluorescent imaging capability of the probe, U87-MG cells with over expressed integrin $\alpha_v\beta_3$ on the cell surface and MCF-7 cells with few integrin $\alpha_v\beta_3$ were incubated with bio-modified Fe_3O_4@Au NPs, respectively. Then the fluorescence of fixed cells was detected by confocal microscopy. In Fig. 6A and B, high fluorescence signals are observed in U87-MG cells, whereas no evident fluorescence is observed in MCF-7 cells. A similar result was demonstrated with the fluorescence histograms obtained using flow cytometry (Fig. 6D).

To further confirm the targeting probe was internalized into cells mainly through the antigen–antibody mediated endocytosis pathway, U87-MG cells were treated with the probe after the cells were incubated with integrin $\alpha_v\beta_3$ mAb. Then the U87-MG cells were detected by confocal microscopy. The fluorescence level detected in the integrin $\alpha_v\beta_3$ mAb-treated group was significantly lower than that in the untreated group, indicating that the targeting effect of the probe was significantly blocked by integrin $\alpha_v\beta_3$ mAb. And the result was confirmed by the fluorescence histograms (Fig. 6D). Effective and specific internalization of the biomodified Fe_3O_4@Au NPs suggested that these probes could be used for targeting and fluorescence imaging.

Every single imaging modality mentioned above possesses characteristic strengths and weaknesses, so they have different advantages in tumor diagnosis. For example, MRI offers the deepest tissue images, which makes it suitable for fundamental detection, but it cannot be used in patients with most forms of medical or biostimulation implants.[53] Fluorescent imaging provides the highest signal sensitivity and is suitable for accurate localization and detection. While photoacoustic imaging and microwave-induced thermoacoustic tomography, which have both deep tissue images and high sensitivity, are also useful for detection of tumors. Clinically, tumors are normally detected without knowing their size, location and depth, so we have to detect them with various imaging modalities to meet different situations, respectively. As a result, various contrast agents have to be injected, which is time-consuming and painful for patients. However, when we use multimodal imaging probes, only one injection is sufficient to complete various imaging modalities and acquire complementary information and accurate diagnosis. The EPR effect allows the nanoparticle-based agents to have a better permeability and retention of tumor tissues than small-molecule contrast agents.[27,46] The PEG-immobilized on them further increases the imaging time to make the multimodal imaging possible.[43] As reported, various pegylated Au NPs have long circulation time to guarantee the multimodal imaging. The pegylated hollow gold nanospheres have elimination half-lives of 71.82 ± 30.46 hours.[54] The pegylated Au NPs of 20 nm have a retention time in blood more than 20 hours and that in tumor is even more than 48 hours.[21] Therefore we estimate that the bio-modified Fe_3O_4@Au NPs will remain in the tumor interstitium for a long time to guarantee the imaging effect of multimodal imaging.

Due to the versatile properties of Au NPs and Fe_3O_4 NPs, Fe_3O_4/Au hybrid nanoparticles of various shapes have been used as multimodal contrast agents for MRI, photoacoustic imaging and magnetomotive photoacoustic imaging.[7,18,19] In our study, Fe_3O_4@Au NPs were used as multimodal contrast agents for MRI, microwave-induced thermoacoustic imaging and photoacoustic imaging. We also modified the Fe_3O_4@Au NPs with fluorescent dye and cancer cell targeted-molecule. So the bio-modified Fe_3O_4@Au NPs can also be used for fluorescence imaging and targeting of cancer cells. The ability of targeting tumor means that the imaging probes are internalized into cancer cells selectively and sensitively. Then a better imaging effect can be achieved with fewer and less severe side effects. The bio-modified Fe_3O_4@Au NPs were conjugated with integrin $\alpha_v\beta_3$

Published on 09 November 2011 on http://pubs.rsc.org | doi:10.1039/C1JM13692E
Downloaded by Xiamen University on 13 December 2011

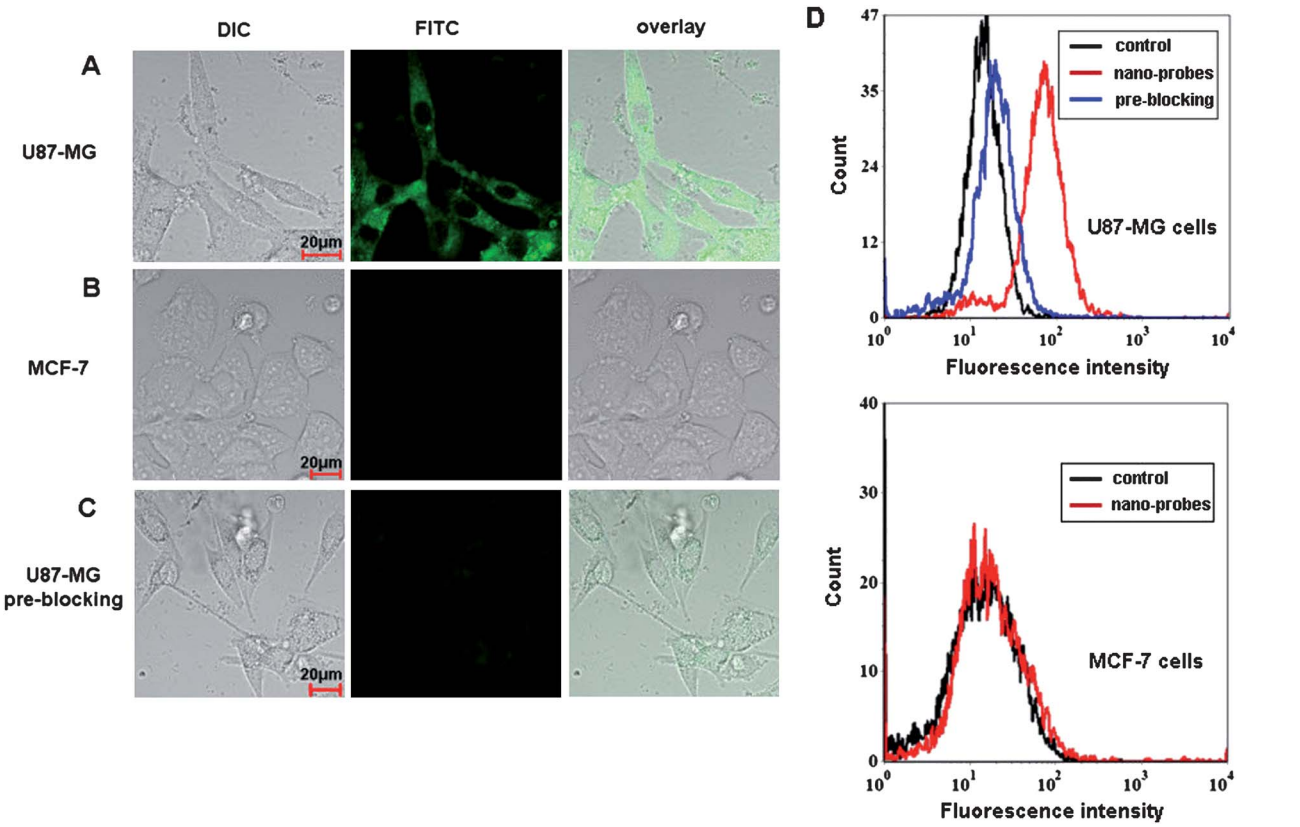

Fig. 6 Confocal images of U87-MG (A), MCF-7 (B) and U87-MG cells pre-blocked by integrin $\alpha_v\beta_3$ mAb (C) incubated with bio-modified Fe_3O_4@Au NPs; (D) fluorescence histograms of U87-MG cells and MCF-7 cells under different treatments.

mAb for targeting cancer cells in this study. But other tumor-targeted molecules can be also connected with Fe_3O_4@Au NPs in the same way if necessary.

Conclusions

In conclusion, Fe_3O_4@Au NPs were synthesized and developed as a novel tumor targeted contrast probe for multimodal imaging after they were modified with antibody and fluorescent dye. As the bio-modified Fe_3O_4@Au NPs generate enhanced MR contrast, they can be used as a contrast agent for T_2 weighed MRI. They also have high photoacoustic and microwave-induced thermoacoustic signals, thus they are useful for both microwave induced thermoacoustic tomography and photo-acoustic imaging. In addition, they can be used for specifically targeting and fluorescent imaging of integrin $\alpha_v\beta_3$-positive cancer cells with FITC-labeled integrin $\alpha_v\beta_3$ mAb. Consequently, the bio-modified Fe_3O_4@Au NPs can be used as a tumor-targeted probe for multimodal imaging and lead to significant development in cancer therapy, as they are broadly applicable for cancer imaging applications. Their multifunctional imaging of tumor *in vivo* and other applications will be presented in our further studies.

Notes and references

1 J. S. Xu, J. Huang, R. Qin, G. H. Hinkle, S. P. Povoski, E. W. Martin and R. X. Xu, *Biomaterials*, 2010, **31**, 1716–1722.
2 B. Sitharaman, K. R. Kissell, K. B. Hartman, L. A. Tran, A. Baikalov, I. Rusakova, Y. Sun, H. A. Khant, S. J. Ludtke, W. Chiu, S. Laus, E. Toth, L. Helm, A. E. Merbach and L. J. Wilson, *Chem Commun*, 2005, 3915–3917.
3 S. Ahn, S. Y. Jung, J. P. Lee, H. K. Kim and S. J. Lee, *ACS Nano*, 2010, **4**, 3753–3762.
4 P. Diagaradjane, A. Deorukhkar, J. G. Gelovani, D. M. Maru and S. Krishnan, *ACS Nano*, 2010, **4**, 4131–4141.
5 J. Kim, Y. Piao and T. Hyeon, *Chem. Soc. Rev.*, 2009, **38**, 372–390.
6 H. Y. Ko, K. J. Choi, C. H. Lee and S. Kim, *Biomaterials*, 2011, **32**, 1130–1138.
7 Y. Jin, C. Jia, S. W. Huang, M. O'Donnell and X. Gao, *Nat. Commun.*, 2010, **1**, 41.
8 B. Chen, H. Zhang, C. Zhai, N. Du, C. Sun, J. Xue, D. Yang, H. Huang, B. Zhang, Q. Xie and Y. Wu, *J. Mater. Chem.*, 2010, **20**, 9895.
9 H.-K. Kim, H.-Y. Jung, J.-A. Park, M.-I. Huh, J.-C. Jung, Y. Chang and T.-J. Kim, *J. Mater. Chem.*, 2010, **20**, 5411.
10 M. Kačenka, O. Kaman, J. Kotek, L. Falteisek, J. Černý, D. Jirák, V. Herynek, K. Zacharovová, Z. Berková, P. Jendelová, J. Kupčík, E. Pollert, P. Veverka and I. Lukeš, *J. Mater. Chem.*, 2011, **21**, 157.
11 D. K. Kirui, D. A. Rey and C. A. Batt, *Nanotechnology*, 2010, **21**, 105105.
12 S. T. Selvan, P. K. Patra, C. Y. Ang and J. Y. Ying, *Angew. Chem.*, 2007, **119**, 2500–2504.
13 W. J. M. Mulder, G. J. Strijkers, G. A. F. van Tilborg, A. W. Griffioen and K. Nicolay, *NMR Biomed.*, 2006, **19**, 142–164.
14 J. Yang, E.-K. Lim, H. J. Lee, J. Park, S. C. Lee, K. Lee, H.-G. Yoon, J.-S. Suh, Y.-M. Huh and S. Haam, *Biomaterials*, 2008, **29**, 2548–2555.
15 P. Sharma, S. C. Brown, N. Bengtsson, Q. Zhang, G. A. Walter, S. R. Grobmyer, S. Santra, H. Jiang, E. W. Scott and B. M. Moudgil, *Chem. Mater.*, 2008, **20**, 6087–6094.
16 F. Bertorelle, C. Wilhelm, J. Roger, F. Gazeau, C. Menager and V. Cabuil, *Langmuir*, 2006, **22**, 5385–5391.

 This journal is © The Royal Society of Chemistry 2012

Published on 09 November 2011 on http://pubs.rsc.org | doi:10.1039/C1JM13692E
Downloaded by Xiamen University on 13 December 2011

17 L. Moriggi, C. Cannizzo, E. Dumas, C. R. Mayer, A. Ulianov and L. Helm, *J. Am. Chem. Soc.*, 2009, **131**, 10828–10829.
18 C. Wang, J. Chen, T. Talavage and J. Irudayaraj, *Angew. Chem., Int. Ed.*, 2009, **48**, 2759–2763.
19 C. Xu, J. Xie, D. Ho, C. Wang, N. Kohler, E. G. Walsh, J. R. Morgan, Y. E. Chin and S. Sun, *Angew. Chem., Int. Ed.*, 2008, **47**, 173–176.
20 S. Hirn, M. Semmler-Behnke, C. Schleh, A. Wenk, J. Lipka, M. Schäffler, S. Takenaka, W. Möller, G. Schmid and U. Simon, *Eur. J. Pharm. Biopharm.*, 2011, **77**, 407–416.
21 G. Zhang, Z. Yang, W. Lu, R. Zhang, Q. Huang, M. Tian, L. Li, D. Liang and C. Li, *Biomaterials*, 2009, **30**, 1928–1936.
22 S. Laurent, D. Forge, M. Port, A. Roch, C. Robic, L. Vander Elst and R. N. Muller, *Chem. Rev.*, 2008, **108**, 2064–2110.
23 P.-J. Chen, S.-H. Hu, C.-S. Hsiao, Y.-Y. Chen, D.-M. Liu and S.-Y. Chen, *J. Mater. Chem.*, 2011, **21**, 2535.
24 L. Nie, Z. Ou, S. Yang and D. Xing, *Med. Phys.*, 2010, **37**, 4193–4200.
25 D. A. Giljohann, D. S. Seferos, W. L. Daniel, M. D. Massich, P. C. Patel and C. A. Mirkin, *Angew. Chem., Int. Ed.*, 2010, **49**, 3280–3294.
26 R. Popovtzer, A. Agrawal, N. A. Kotov, A. Popovtzer, J. Balter, T. E. Carey and R. Kopelman, *Nano Lett.*, 2008, **8**, 4593–4596.
27 H. Maeda, *Adv. Enzyme Regul.*, 2001, **41**, 189–207.
28 M. Wang and M. Thanou, *Pharmacol. Res.*, 2010, **62**, 90–99.
29 L. Brannon-Peppas and J. O. Blanchette, *Adv. Drug Delivery Rev.*, 2004, **56**, 1649–1659.
30 J. D. Byrne, T. Betancourt and L. Brannon-Peppas, *Adv. Drug Delivery Rev.*, 2008, **60**, 1615–1626.
31 P. Pouponneau, J. C. Leroux, G. Soulez, L. Gaboury and S. Martel, *Biomaterials*, 2011, **32**, 3481–3486.
32 R. J. Lee and P. S. Low, *J. Biol. Chem.*, 1994, **269**, 3198–3204.
33 Z. M. Qian, H. Li, H. Sun and K. Ho, *Pharmacol. Rev.*, 2002, **54**, 561–587.
34 H. Liu, A. K. Rajasekaran, P. Moy, Y. Xia, S. Kim, V. Navarro, R. Rahmati and N. H. Bander, *Cancer Res.*, 1998, **58**, 4055–4060.
35 G. R. Reddy, M. S. Bhojani, P. McConville, J. Moody, B. A. Moffat, D. E. Hall, G. Kim, Y. E. Koo, M. J. Woolliscroft, J. V. Sugai, T. D. Johnson, M. A. Philbert, R. Kopelman, A. Rehemtulla and B. D. Ross, *Clin. Cancer Res.*, 2006, **12**, 6677–6686.
36 A. S. Arbab, L. A. Bashaw, B. R. Miller, E. K. Jordan, B. K. Lewis, H. Kalish and J. A. Frank, *Radiology*, 2003, **229**, 838–846.
37 M. J. Glennie and J. G. van de Winkel, *Drug Discovery Today*, 2003, **8**, 503–510.
38 A. J. Beer and M. Schwaiger, *Cancer Metastasis Rev.*, 2008, **27**, 631–644.
39 W. Cai, S. Sam Gambhir and X. Chen, *BioTechniques*, 2005, **39**, S14–S25.
40 J. L. Lyon, D. A. Fleming, M. B. Stone, P. Schiffer and M. E. Williams, *Nano Lett.*, 2004, **4**, 719–723.
41 Z. Ou, B. Wu, D. Xing, F. Zhou, H. Wang and Y. Tang, *Nanotechnology*, 2009, **20**, 105102.
42 L. Xiang, Y. Yuan, D. Xing, Z. Ou, S. Yang and F. Zhou, *J. Biomed. Opt.*, 2009, **14**, 021008.
43 J. M. Harris, N. E. Martin and M. Modi, *Clin. Pharmacokinet.*, 2001, **40**, 539–551.
44 W. E. Doering, M. E. Piotti, M. J. Natan and R. G. Freeman, *Adv. Mater.*, 2007, **19**, 3100–3108.
45 J. H. Lee, Y. M. Huh, Y. W. Jun, J. W. Seo, J. T. Jang, H. T. Song, S. Kim, E. J. Cho, H. G. Yoon, J. S. Suh and J. Cheon, *Nat. Med.*, 2007, **13**, 95–99.
46 H. Yang, Y. Zhuang, Y. Sun, A. Dai, X. Shi, D. Wu, F. Li, H. Hu and S. Yang, *Biomaterials*, 2011, **32**, 4584–4593.
47 R. A. Kruger, D. R. Reinecke and G. A. Kruger, *Med. Phys.*, 1999, **26**, 1832–1837.
48 X. Yang, S. E. Skrabalak, Z. Y. Li, Y. Xia and L. V. Wang, *Nano Lett.*, 2007, **7**, 3798–3802.
49 L. V. Wang, *Nat. Photonics*, 2009, **3**, 503–509.
50 S. Mallidi, T. Larson, J. Tam, P. P. Joshi, A. Karpiouk, K. Sokolov and S. Emelianov, *Nano Lett.*, 2009, **9**, 2825–2831.
51 S. Mallidi, T. Larson, J. Aaron, K. Sokolov and S. Emelianov, *Opt. Express*, 2007, **15**, 6583–6588.
52 W. M. Leevy, S. T. Gammon, H. Jiang, J. R. Johnson, D. J. Maxwell, E. N. Jackson, M. Marquez, D. Piwnica-Worms and B. D. Smith, *J. Am. Chem. Soc.*, 2006, **128**, 16476–16477.
53 C. Jost and V. V. Kumar, *J. Invasive. Cardiol.*, 1998, **10**, 477–479.
54 W. Lu, Q. Huang, G. Ku, X. Wen, M. Zhou, D. Guzatov, P. Brecht, R. Su, A. Oraevsky, L. V. Wang and C. Li, *Biomaterials*, 2010, **31**, 2617–2626.

Addition and correction

Bio-modified Fe_3O_4 core/Au shell nanoparticles for targeting and multimodal imaging of cancer cells

Ting Zhou, Baoyan Wu and Da Xing

J. Mater. Chem., 2012, **22**, 470-477 (DOI: 10.1039/C1JM13692E).

The following acknowledgements section should be included in the article:

Acknowledgements
This research is supported by the National Basic Research Program of China (2011CB910402; 2010CB732602), the Key Program of NSFC-Guangdong Joint Funds of China (U0931005), and the Program for Changjiang Scholars and Innovative Research Team in University (IRT0829). We are also grateful to Dr Huan Qin for the help with thermoacoustic experiments, to Dr Yi Yuan for the help with photoacoustic experiments, to Professor Quan Zhou for the help with MRI, to Dr Xiaoming Zhou and Dr Sihua Yang for much good advice to this work.

The Royal Society of Chemistry apologises for these errors and any consequent inconvenience to authors and readers.

Additions and corrections can be viewed online by accessing the original article to which they apply.

This journal is © The Royal Society of Chemistry 2011